Hepatocellular Carcinoma: Signal Intensity at Gadoxetic Acid–enhanced MR Imaging—Correlation with Molecular Transporters and Histopathologic Features[1]

Azusa Kitao, MD
Yoh Zen, MD
Osamu Matsui, MD
Toshifumi Gabata, MD
Satoshi Kobayashi, MD
Wataru Koda, MD
Kazuto Kozaka, MD
Norihide Yoneda, MD
Tatsuya Yamashita, MD
Shuichi Kaneko, MD
Yasuni Nakanuma, MD

Purpose: To analyze the correlation between signal intensity in the hepatobiliary phase of gadoxetic acid–enhanced magnetic resonance (MR) imaging and the expression of hepatocyte transporters with histopathologic features in hepatocellular carcinoma (HCC).

Materials and Methods: Institutional ethics committee approval and informed consent were obtained. Forty surgically resected HCCs were classified as hypointense (n = 32) or iso- or hyperintense (n = 8) on the basis of findings in the hepatobiliary phase of gadoxetic acid–enhanced MR imaging. The following were compared between hypointense and iso- or hyperintense HCCs: the time–signal intensity curves at gadoxetic acid–enhanced MR imaging, the expression levels of seven transporters (four organic anion–transporting polypeptides [OATPs] and three multidrug-resistant proteins [MRPs]) at polymerase chain reaction (PCR) (for 22 nodules), results of immunostaining of OATP8, and histologic features. Statistical analysis (unpaired t test, Mann-Whitney test, χ^2 test, and Fisher exact test) was performed for each result.

Results: On the time–signal intensity curves, hypointense HCCs showed a decreasing pattern, whereas iso- or hyperintense HCCs showed an increasing pattern after the dynamic phase. PCR revealed that expression of OATP8 (an uptake transporter) in hypointense HCCs was lower and that in iso- or hyperintense HCCs was higher than in background liver ($P < .001$). The expression level of MRP3 (a sinusoidal export transporter) showed a similar trend to that of OATP8 ($P < .001$). Immunostaining revealed that OATP8 expression was weak in hypointense HCCs, whereas it was sustained in iso- or hyperintense HCCs ($P < .001$). At histologic examination, a pseudoglandular proliferation pattern with bile plugs was more commonly observed in iso- or hyperintense HCCs than in hypointense HCCs ($P = .01$ for proliferation patterns and $P = .006$ for bile plugs).

Conclusion: The enhancement ratio of HCCs in the hepatobiliary phase of gadoxetic acid–enhanced MR imaging positively correlated with expression levels of OATP8 and MRP3, indicating that gadoxetic acid is taken up by OATP8 and excreted by MRP3.

Supplemental material: *http://radiology.rsna.org/lookup/suppl/doi:10.1148/radiol.10092214/-/DC1*

[1] From the Departments of Radiology (A.K., O.M., T.G., S. Kobayashi, W.K., K.K., N.Y.), Human Pathology (A.K., Y.Z., Y.N.), and Gastroenterology (T.Y., S. Kaneko), Kanazawa University Graduate School of Medical Science, 13-1 Takara-machi, Kanazawa 920-8640, Japan. Received November 24, 2009; revision requested January 6, 2010; revision received February 25; accepted March 24; final version accepted April 28. Supported in part by a Grant-in-Aid for Scientific Research (no. 21591549) from the Ministry of Education, Culture, Sports, Science and Technology, Tokyo, Japan and by Japanese Health and Labor Sciences research grants for the development of novel molecular markers and imaging modalities for earlier diagnosis of hepatocellular carcinoma. **Address correspondence to** A.K. (e-mail: *kitao@rad.m.kanazawa-u.ac.jp*).

Gadoxetic acid is a recently developed hepatobiliary-specific contrast material for magnetic resonance (MR) imaging that has high sensitivity in the detection of malignant liver tumors (1–7). Because gadoxetic acid is taken up by hepatocytes and then excreted into the bile ducts (8), hepatic focal lesions without normal hepatobiliary function can be definitively depicted as hypointense areas compared with the well-enhanced hyperintense background liver in the hepatobiliary phase of gadoxetic acid–enhanced MR imaging (1,9). In addition, gadoxetic acid can be used in the same way as gadopentetate dimeglumine to evaluate the hemodynamics of hepatic lesions in the dynamic phase after an intravenous bolus injection (1,2,4–6).

Classically, hepatocellular carcinomas (HCCs) commonly show rapid enhancement in the arterial dominant phase and a decrease in signal intensity (SI) from the portal dominant phase to the equilibrium phase. This decreasing pattern corresponds to the decline of contrast material in the tumor blood spaces, or so-called washout (10). In the hepatobiliary phase of gadoxetic acid–enhanced MR imaging, most HCCs are hypointense, although hyperintense HCCs are also sometimes encountered (4,7). Elucidating the mechanisms of this difference in imaging appearance may be important in the detection and characterization of HCCs. However, the uptake and excretion of gadoxetic acid in human liver and hepatic tumors have not been well analyzed (11,12).

In a rat experimental study, the hepatic uptake transporter of gadoxetic acid was confirmed to be organic anion–transporting polypeptide (OATP) 1 (13), and the export transporter was multidrug-resistant protein (MRP) 2 (14). However, the results obtained in rats cannot necessarily be easily applied to humans. Substrates transported by rat OATP1 can be taken up by OATP-A, OATP-B, OATP-C, and OATP8, which are also expressed on the sinusoidal side of human hepatocytes (15–20). Regarding export transporters, MRP2 in rat liver is considered to be an homologue to MRP2 in human liver, which is expressed on the canalicular side of hepatocytes (21–23). In addition, MRP1 and MRP3 on the sinusoidal side of human hepatocytes can also export some of the substrates of MRP2 (22,24). These seven transporters carry organic anions containing many kinds of intrinsic or extrinsic molecules—for example, a component of bile acid, hormones, and several drugs (15–24). Gadoxetic acid is also an organic anion, and therefore we expected that some of those transporters would be involved in the uptake and excretion of this contrast material in human liver and HCCs.

We performed this study to analyze the correlation between SI in the hepatobiliary phase of gadoxetic acid–enhanced MR imaging and the expression of hepatocyte transporters with histopathologic features in HCC.

Advances in Knowledge

- The expressions of the hepatocyte membrane uptake transporter organic anion–transporting polypeptide 8 (OATP8) and the export transporter multidrug-resistant protein 3 (MRP3) significantly correlate with the signal intensity of hepatocellular carcinomas (HCCs) in the hepatobiliary phase of gadoxetic acid–enhanced MR imaging ($P < .001$).
- On human HCC cells, OATP8 and MRP3 are the most probable uptake transporter and export transporter of gadoxetic acid, respectively.
- At histologic examination, a pseudoglandular proliferation pattern with bile plugs was observed with significantly high frequency in HCCs that were iso- or hyperintense in the hepatobiliary phase of gadoxetic acid–enhanced MR imaging ($P < .01$).
- The time–signal intensity curve of HCCs at gadoxetic acid–enhanced MR imaging can differ between hypointense HCCs and iso- or hyperintense HCCs ($P < .001$).

Implication for Patient Care

- When we encounter iso- or hyperintense HCCs in the hepatobiliary phase of gadoxetic acid–enhanced MR imaging, we can speculate that the pathologic examination will show a pseudoglandular proliferation pattern and bile plugs.

Materials and Methods

Patients

This retrospective study was performed with the approval of the institutional ethics committee, and informed consent for use of the MR images and the resected specimens was obtained from all patients. Forty-nine HCCs in 47 patients were surgically resected at our institution from April 2008 to June 2009. We excluded nine HCCs in nine patients, including three patients who did not undergo gadoxetic acid–enhanced MR imaging because of renal failure and three patients with a history of previous treatment for HCC, including ablation therapy or transarterial chemoembolization therapy. One pathologist (Y.Z., with 11 years of experience) and one abdominal imaging radiologist (A.K., with 8 years of experience) evaluated and excluded three HCCs with necrosis, hemorrhage, and/or cystic degeneration

Published online before print
10.1148/radiol.10092214

Radiology 2010; 256:817–826

Abbreviations:
HCC = hepatocellular carcinoma
MRP = multidrug-resistant protein
OATP = organic anion–transporting polypeptide
PCR = polymerase chain reaction
ROI = region of interest
SI = signal intensity

Author contributions:
Guarantors of integrity of entire study, A.K., O.M., T.G., S. Kaneko, Y.N.; study concepts/study design or data acquisition or data analysis/interpretation, all authors; manuscript drafting or manuscript revision for important intellectual content, all authors; manuscript final version approval, all authors; literature research, A.K.; clinical studies, A.K., O.M., T.G., S. Kobayashi, W.K., K.K., T.Y.; experimental studies, A.K., Y.Z., N.Y., T.Y., S. Kaneko, Y.N.; statistical analysis, A.K.; and manuscript editing, A.K., Y.Z., O.M., Y.N.

Authors stated no financial relationship to disclose.

See also the article by Tsuda and Matsui in this issue.

covering more than one-fourth of the entire lesion at histologic examination. Therefore, our final study comprised 40 HCCs in 38 patients. Mean patient age was 63.0 years ± 10.4 (standard deviation) (range, 38–81 years) for the entire study group, 63.0 years ± 11.0 (range, 38–81 years) for men, and 63.0 years ± 9.4 (range, 43–78 years) for women. The male:female ratio was 26:12 (68%:32%), and 34 (89%) of 38 patients had chronic liver disease (Table 1). Hepatic function was preserved in all patients, and all patients with liver cirrhosis had grade A cirrhosis according to the Child classification.

Table 1

Clinical Features of Patients

Feature	Hypointense HCC	Iso- or Hyperintense HCC
No. of tumors	32	8
Resected tumor size (cm)	4.2 ± 2.9 (0.7–14.5)	4.0 ± 2.9 (2.2–10.5)
Age (y)	61.8 ± 10.3 (38–78)	66.0 ± 10.8 (51–81)
Male-to-female ratio*	22:10	6:2
Background liver tissue*		
Chronic hepatitis	9 (One patient with HBV, six with HCV, and two with cryptogenic hepatitis)	2 (Both patients had HCV)
Liver cirrhosis	18 (Four patients with HBV, nine with HCV, two with NASH, one with AIH, and two with cryptogenic cirrhosis)	5 (One patient with HBV, one with HCV, two with NASH, and one with cryptogenic cirrhosis)
Normal liver	5	1

Note.—Unless otherwise specified, data are means ± standard deviations, with ranges in parentheses. No significant differences were observed in any clinical features between the two types of HCCs (size: $P = .84$; age: $P = .32$; sex: $P > .99$; background liver: $P = .95$. AIH = autoimmune hepatitis, HBV = hepatitis B virus, HCV = hepatitis C virus, NASH = nonalcoholic steatohepatitis.

* Data are numbers of patients.

Gadoxetic Acid–enhanced MR Imaging

Gadoxetic acid–enhanced MR imaging was performed before surgical resection (mean time before surgery, 52.8 days ± 25.3 [range, 3–95 days]) for the characterization and pretreatment staging of HCC. MR images were obtained with either a 1.5-T (n = 15) or 3.0-T (n = 25) MR system (Signa HDx; GE Medical Systems, Milwaukee, Wis) by using the same protocol. MR imaging was performed with a fat-suppressed three-dimensional T1-weighted spoiled gradient echo in the steady state sequence (liver acquisition with volume acceleration extended version, generalized encoding matrix; repetition time msec/echo time msec, 3.4–3.6/1.6; flip angle, 12°–15°; field of view, 42 × 42 cm; matrix, 192 × 320 interpolated to 512 × 512; section thickness, 4.2 mm; and overlap, 2.1 mm). For the dynamic study, a dose of 0.1 mL of Primovist (0.25 mmol/mL of gadoxetic acid, Bayer Schering Pharma, Berlin, Germany) per kilogram of body weight was intravenously injected at a flow rate of 1.0 mL/sec (25), followed by a 30-mL saline flush. We used the test injection method (1.5 mL of gadoxetic acid plus an 8-mL saline flush) to determine the optimal arterial dominant phase, which was determined as the peak time of enhancement in the abdominal aorta plus an additional 10 seconds of imaging time (16–22 seconds) · ½. After imaging in the arterial phase, portal phase and equilibrium phase images were obtained 20 and 60 seconds after the previous imaging phase was finished, respectively. The hepatobiliary phase was imaged 20 minutes after the injection in all patients. In 27 patients, imaging was performed in an additional phase 15 minutes after the injection.

Analysis of SI on Gadoxetic Acid–enhanced MR Images

Image analysis was performed in consensus by two abdominal imaging radiologists (A.K. and O.M. [with 38 years of experience]). The SIs of the tumor and surrounding background liver were measured by placing regions of interest (ROIs). The ROI of the tumor was determined as the maximum oval or round area at the level of the largest diameter of the tumor, and the average ROI size was 923.6 mm² ± 1418.3 (range, 61–6167 mm²). For both nodules with homogeneous SI and nodules with heterogeneous SI, the average intensity of the entire area was used for analysis. A similarly sized ROI was set over the adjacent liver parenchyma, avoiding the large vessels. ROIs were measured in the arterial, venous, equilibrium, and delayed phases.

Classification of HCCs in the Hepatobiliary Phase of Gadoxetic Acid–enhanced MR Imaging

The HCC nodules were retrospectively classified into two types according to the SI measurement in the hepatobiliary phase of gadoxetic acid–enhanced MR imaging—namely, hypointense HCCs and iso- or hyperintense HCCs. Hypointense HCCs had lower SIs (tumor SI/background SI < 0.9) in the hepatobiliary phase (Fig 1a; Fig E1 [online]). Iso- or hyperintense HCCs had the same or higher SIs (tumor SI/background SI ≥ 1.0) (Fig 1b). There was no intermediate case (tumor SI/background SI = 0.9–1.0). In this study, all HCCs demonstrated hypointensity relative to the surrounding liver on precontrast T1-weighted images, and therefore all iso- or hyperintense HCCs were considered to be enhanced in the hepatobiliary phase of gadoxetic acid–enhanced MR imaging.

Time-SI Curve at Gadoxetic Acid–enhanced MR Imaging

To assess the degree and time course of gadoxetic acid uptake and/or export, we measured the SI at the maximum cross section of each ROI in the precontrast, arterial, portal, equilibrium, and hepatobiliary phases. We calculated the enhancement ratio [(postenhancement SI minus pre-enhancement SI)/pre-enhancement SI] at each time point and traced time-SI curves with software (Prism5; GraphPad Software, San Diego, Calif). One radiologist (A.K.) performed this analysis.

Histologic Diagnosis

Hematoxylin-eosin staining of tissue slices was performed for all 40 liver specimens.

Figure 1

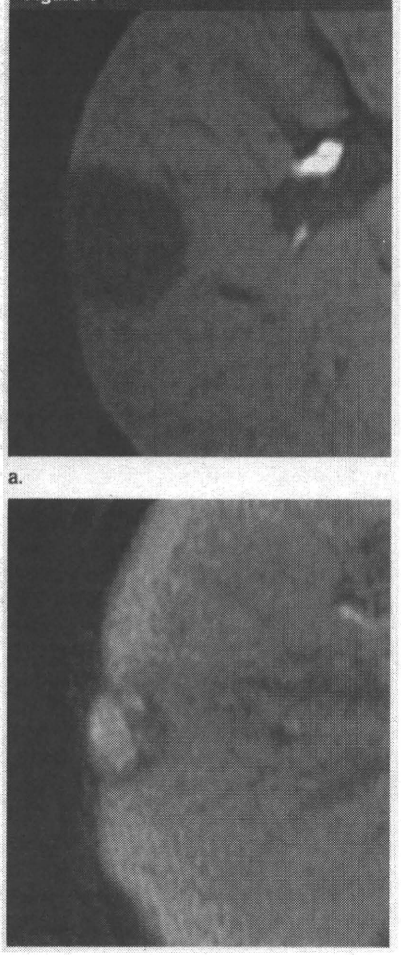

a.

b.

Figure 1: Typical findings of the two types of HCC in the hepatobiliary phase of gadoxetic acid–enhanced axial MR imaging. **(a)** On image obtained in the hepatobiliary phase (20 minutes after injection of gadoxetic acid) in a 62-year-old woman, a hypointense HCC shows definitely lower SI. **(b)** In contrast, image of iso- or hyperintense HCC obtained in 66-year-old man shows almost higher SI, with a portion showing lower SI relative to the surrounding enhanced liver.

Two pathologists (Y.Z. and Y.N. [with 37 years of experience]) diagnosed each nodule according to the classification proposed by the International Working Party (26) and the World Health Organization classification (27): well, moderately, or poorly differentiated HCC. Then, HCCs were classified into four proliferative patterns—namely, trabecular, pseudoglandular, solid, and scirrhous patterns. We compared hypointense HCCs and iso- or hyperintense HCCs with regard to histologic features such as tumor differentiation, proliferation pattern, and the presence of bile plugs.

Polymerase Chain Reaction Analysis

The expression of OATP-A, OATP-B, OATP-C, OATP8, MRP1, MRP2 and MRP3 messenger RNA was examined by means of reverse transcription polymerase chain reaction (PCR) in HCCs and the surrounding liver tissue in 22 livers (Table 2) from which we could obtain fresh-frozen specimens. In the remaining 18 livers, the frozen specimens were not preserved. β-Actin was used as an internal reference. Primer sequences and product sizes are shown in Table E1 (online).

Next, we quantitatively examined messenger RNA expression levels of seven transporters in the same 22 livers by using real-time PCR. Specific primers and probes for seven transporters and β-actin were obtained from Applied Biosystems (Warrington, England). For quantitative evaluation of the expression of each transporter, we used the tumor/background expression score, defined as (tumor transporter value/tumor β-actin value)/(background transporter value/background β-actin value). Then, we examined the correlation of the transporter expression score and the enhancement ratio in the hepatobiliary phase of gadoxetic acid–enhanced MR imaging.

Immunohistochemical Analysis

According to the results of reverse transcription PCR, which indicated that OATP8 would be the key uptake transporter, immunostaining of OATP8 was performed for all HCCs by using a primary antibody against human OATP8 (mouse monoclonal, NB100–74482; Novus Biologicals, Littleton, Colo) (1:100). After removal of the specimen from the paraffin, antigen retrieval was performed by microwaving it in an edetic acid buffer (pH, 8.0) for 20 minutes. Two abdominal imaging radiologists (A.K. and N.Y. [with 7 years of experience]) semiquantitatively evaluated the intensity of OATP8 expression on the tumor cellular membrane in comparison with that of nonneoplastic hepatocytes as follows: A grade of 0 indicated no expression; a grade of 1+, decreased expression; a grade of 2+, equivalent expression; and a grade of 3+, increased expression. We used the grade at the largest area of each nodule.

Dual immunofluorescence staining of OATP8 and coagulation factor VIII, a marker of endothelial cells, was performed to examine whether or not OATP8 is expressed on the sinusoidal side of carcinoma cells. We used the previously described antibody for human OATP8 and rabbit polyclonal antibody for human factor VIII (A0082; Dako Cytomation, Glostrup, Denmark).

The details of the experiments (reverse transcription PCR and immunostaining) were as described in the article by Nakamura et al (28).

Overall Assessment

A schematic for the molecular background of the dynamics of gadoxetic acid in HCC cells as considered from our study was developed.

Statistical Analysis

Statistical significance was evaluated with software (Prism5; GraphPad Software, San Diego, Calif). The unpaired *t* test was used for the analysis of clinical features and quantitative reverse transcription PCR results, the Fisher exact test and the χ^2 test were used for the analysis of clinical and histologic features, the Friedman test was used for the time-SI curve, the Mann-Whitney test was used for the immunohistochemical findings, and the Pearson correlation test was used for the correlations between quantitative reverse transcription PCR and the enhancement ratio. $P < .05$ was considered to indicate a statistically significant difference.

Results

Clinical Features of the Two Types of HCCs

Thirty-two nodules were classified as hypointense HCCs, and eight nodules

Figure 2

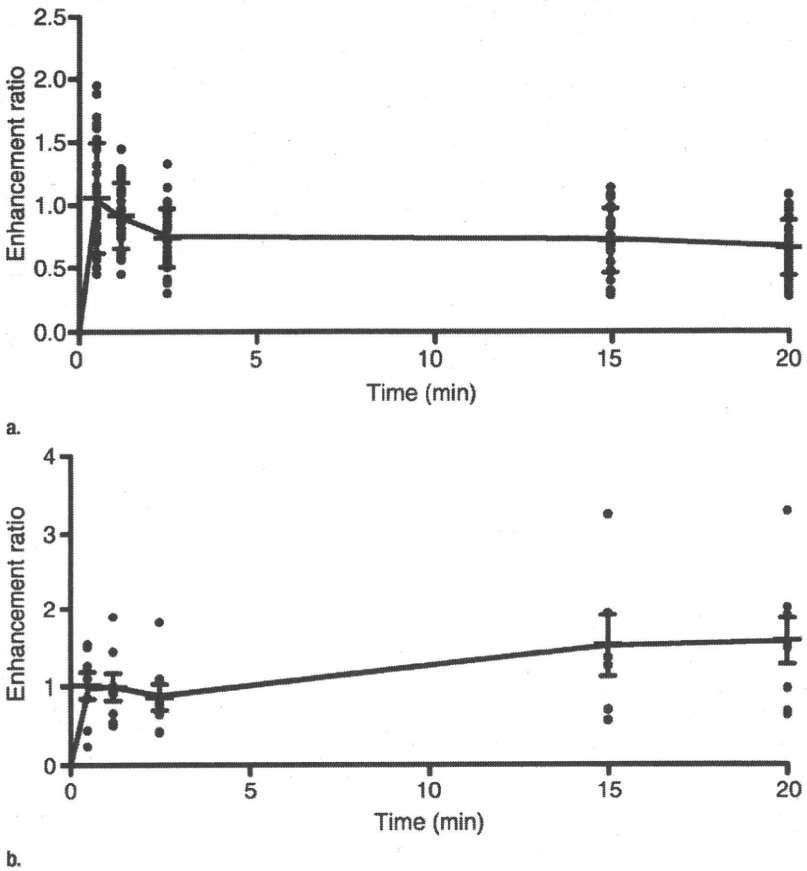

Figure 2: Time-SI curves at gadoxetic acid–enhanced MR imaging. Both hypointense HCCs and iso- or hyperintense HCCs show a rapid, increasing pattern in the arterial or the portal phase. **(a)** In hypointense HCCs, enhancement ratio decreases from the equilibrium phase to the hepatobiliary phase. **(b)** In contrast, iso- or hyperintense HCCs show increasing curves from the equilibrium phase to the hepatobiliary phase. $P < .001$. Enhancement ratio = (pre-enhancement SI minus postenhancement SI)/pre-enhancement SI.

were classified as iso- or hyperintense HCCs. No significant differences in any clinical features were observed between the two types (Table 1).

Time-SI Curves at Gadoxetic Acid–enhanced MR Imaging

Both the hypointense HCCs and the iso- or hyperintense HCCs showed a spike-like rapid increase of enhancement ratio in the arterial phase. After the equilibrium phase, the enhancement ratio decreased in hypointense HCCs; in contrast, iso- or hyperintense HCCs showed increasing intensity curves ($P < .001$) (Fig 2).

Messenger RNA Expression of Hepatocyte Membrane Transporters

OATP8 was constantly expressed in the background nonneoplastic portions of the livers. However, its expression was slight in all hypointense HCCs. In contrast, OATP8 expression was evident in all iso- or hyperintense HCCs (Fig 3). According to the results of real-time quantitative reverse transcription PCR (Fig 4; Fig E2 [online]), the degree of OATP8 expression in all hypointense HCCs was less than that in background livers (tumor/background expression score, <1.0), and was higher in iso- or hyperintense HCCs than in background livers (tumor/background expression score, >1.0) ($P < .001$).

The expression of MRP3, an export transporter on the sinusoidal side, was also lower in hypointense HCCs and was preserved in iso- or hyperintense HCCs, with a significant difference ($P < .001$). No significant difference was observed in the expression levels of the other transporters between the two types of HCCs ($P = .07–.53$). MRP2, a major export transporter on the canalicular side, was constantly expressed in all HCCs (Figs 3, 4; Fig E2 [online]).

There was a significant correlation between the tumor/background expression score of OATP8 and enhancement ratio in the hepatobiliary phase of gadoxetic acid–enhanced MR imaging ($P < .001$, $R = 0.84$) (Fig 5).

Immunohistochemistry of OATP8

In the nonneoplastic liver, OATP8 was expressed on the cellular membrane of hepatocytes at the sinusoidal side. In iso- or hyperintense HCCs, OATP8 was similarly expressed on the cellular membrane of HCC cells. In contrast, the degree of OATP8 expression in hypointense HCCs was clearly weaker than that in nonneoplastic liver ($P < .001$) (Figs 6, 7).

At double immunostaining of OATP8 and coagulation factor VIII in iso- or hyperintense HCCs, OATP8 was expressed on the sinusoidal side labeled by factor VIII in iso- or hyperintense HCCs (Fig E3 [online]). That is, in iso- or hyperintense HCCs, OATP8 expression was sustained on the cellular membrane at the sinusoidal side—the same as in nonneoplastic hepatocytes.

Pathologic Features of the Two Types of HCCs

Seven (88%) of eight iso- or hyperintense HCCs were moderately differentiated, and six (75%) of eight showed a predominantly pseudoglandular pattern, while seven (88%) of eight were associated with bile production (bile plugs). On the other hand, the hypointense HCCs consisted of three cases of well-differentiated, 25 cases of moderately differentiated, and four cases of poorly differentiated HCCs; the trabecular proliferation pattern was most

Table 2

Clinical, Histologic, and Radiologic Features in 22 Patients in Whom PCR Data Were Available

Patient Sex/Age (y)	Tumor Size (cm)	Differentiation	Proliferation Pattern	Bile Plugs	Gadoxetic Acid–enhanced MR Imaging Appearance
M/58	3.5	Moderate	Trabecular	Absent	Hypointense
M/77	14.5	Moderate	Pseudoglandular	Present	Hypointense
M/65	2.6	Moderate	Pseudoglandular	Present	Hypointense
M/78	8.8	Moderate	Solid	Absent	Hypointense
F/71	3.0	Moderate	Trabecular	Absent	Hypointense
M/60	2.5	Well	Pseudoglandular	Present	Hypointense
F/63	1.3	Well	Trabecular	Absent	Hypointense
F/60	1.8	Moderate	Trabecular	Absent	Hypointense
M/68	2.0	Well	Trabecular	Absent	Hypointense
M/63	3.8	Moderate	Trabecular	Absent	Hypointense
F/61	9.5	Moderate	Trabecular	Absent	Hypointense
M/60	5.2	Poor	Trabecular	Absent	Hypointense
M/52	7.2	Moderate	Trabecular	Absent	Hypointense
F/75	3.5	Moderate	Trabecular	Absent	Hypointense
F/63	3.3	Moderate	Pseudoglandular	Present	Hypointense
M/61	3.7	Moderate	Trabecular	Absent	Hypointense
M/57	2.0	Moderate	Trabecular	Absent	Hypointense
M/65	2.4	Moderate	Pseudoglandular	Present	Hyperintense
F/52	10.5	Moderate	Pseudoglandular	Present	Hyperintense
M/74	2.5	Well	Trabecular	Absent	Hyperintense
M/66	2.8	Moderate	Pseudoglandular	Present	Hyperintense
M/76	6.0	Moderate	Pseudoglandular	Present	Hyperintense

Figure 3

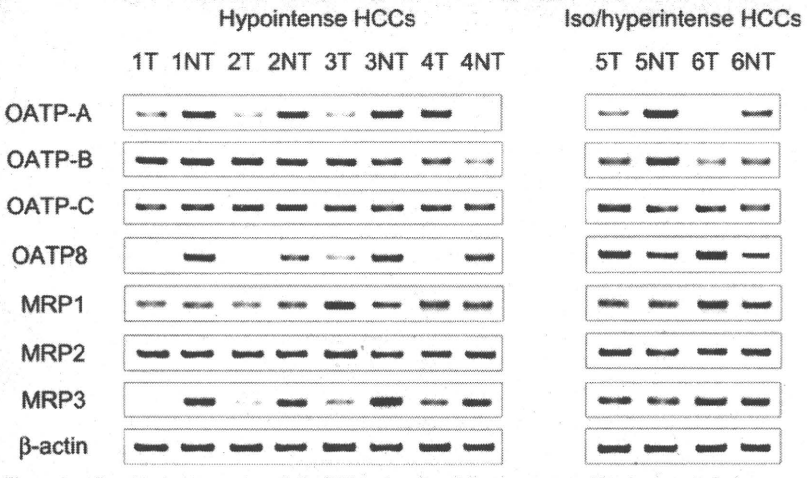

Figure 3: Results of reverse transcription PCR for hepatocellular transporters. Data in six typical cases of HCC are shown; the remaining cases also showed similar results. All transporters are almost constantly expressed in the background nonneoplastic livers. Expression of OATP8, an uptake transporter, is weak in hypointense HCCs (cases 1–4). In contrast, its expression in iso- or hyperintense HCCs is higher than that in background liver (cases 5–6). Expression of MRP3, an export transporter on the sinusoidal side, is also lower in hypointense HCCs and is preserved in iso- or hyperintense HCCs. There are no clear differences in the expression levels of the other five transporters (OATP-A, OATP-B, OATP-C, MRP1, and MRP2) between the two groups. *NT* = nontumor, *T* = tumor.

common (23 [72%] of 32 cases), whereas the pseudoglandular pattern and bile production were also observed in some cases (six [19%] and 10 [31%] cases, respectively). There was no significant difference compared with the occurrence in hypointense HCCs ($P = .57$). In contrast, there were significant differences in proliferation patterns and bile production between the two types of HCCs ($P = .01$ and $P = .006$, respectively) (Fig 8).

Figure 9 shows the molecular background of the dynamics of gadoxetic acid in HCC cells in our study. In iso- or hyperintense HCCs, a large amount of gadoxetic acid would be taken up from the tumor blood sinusoids into HCC cells by OATP8 and be gradually excreted again into tumor blood sinusoids by not MRP2 but MRP3, probably because of the depletion of bile ducts in the HCCs. On the other hand, the uptake of gadoxetic acid might be blocked or reduced because of the lower expression of OATP8 in hypointense HCCs.

Discussion

It has been reported that, uniquely among hepatic malignant tumors, some HCCs show iso- or hyperintensity in the hepatobiliary phase of gadoxetic acid–enhanced MR imaging (4,7). It has been suggested that this is reflective of the degree of residual hepatobiliary function or grade of tumor differentiation (11,12); however, to our knowledge, no basic studies are available to support these contentions. To clarify the mechanism underlying this finding, we performed an imaging-molecular-pathologic correlation study to compare HCCs that were hypointense to surrounding liver with those that were iso- or hyperintense.

Time-SI curves in hypointense HCCs showed a decrease in the SI of the tumor after the dynamic phase that continued to the hepatobiliary phase. This decreasing pattern corresponds to the so-called washout of contrast material from the tumor blood spaces commonly seen in hypervascular HCCs in the equilibrium phase of dynamic MR imaging with gadopentetate dimeglumine (10).

Figure 4

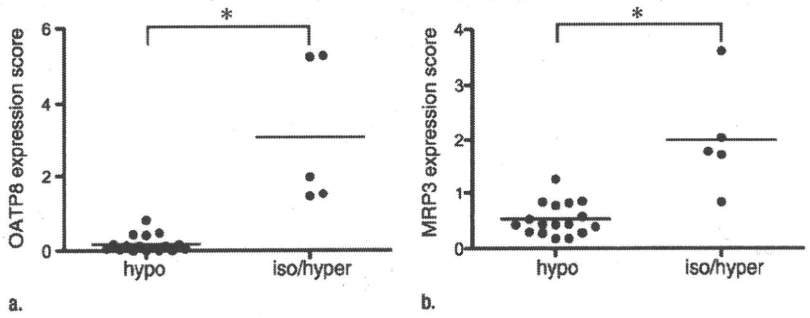

Figure 4: Graphs show results of quantitative real-time PCR of transporters. Hypointense HCCs *(hypo)* have significantly lower expression levels of **(a)** OATP8 and **(b)** MRP3 messenger RNA compared with iso- or hyperintense HCCs *(iso/hyper)* (* = $P < .001$). Expression score = (tumor transporter value/tumor β-actin value)/(background transporter value/background β-actin value). Tumor enhancement ratio = (pre-enhancement SI minus postenhancement SI)/pre-enhancement SI (in hepatobiliary phase).

Figure 5

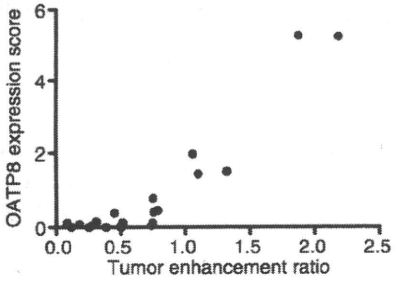

Figure 5: Correlation of OATP8 expression at PCR and tumor enhancement ratio in the hepatobiliary phase. There is a significant correlation between the tumor/background expression score of OATP8 and enhancement ratio in the hepatobiliary phase of gadoxetic acid–enhanced MR imaging. $P < .001$, $R = 0.84$. Expression score = (tumor transporter value/tumor β-actin value)/(background transporter value/background β-actin value). Enhancement ratio = (pre-enhancement SI minus postenhancement SI)/pre-enhancement SI.

This suggests that the decreasing pattern of the curve reflects the decline of the contrast medium in the tumor blood spaces and that the tumor cells hardly take up gadoxetic acid. In contrast, iso- or hyperintense HCCs demonstrated an increasing curve. This indicates that the uptake of gadoxetic acid is greater than the washout in iso- or hyperintense HCCs.

The PCR and immunostaining results showed that the OATP8 expression level was significantly higher in the iso- or hyperintense HCCs and significantly lower in hypointense HCCs than in the surrounding liver. In addition, the OATP8 expression level in HCCs was significantly and positively correlated with the enhancement ratio in the hepatobiliary phase of gadoxetic acid–enhanced MR imaging. Immunostaining also verified the location of OATP8 on the sinusoidal-side membrane of iso- or hyperintense HCC cells—the same as in nonneoplastic hepatocytes. On the basis of these results, we conclude that OATP8 is the best candidate among the four OATPs we tested to help determine the uptake of gadoxetic acid in HCC cells.

An important point is that particularly OATP8 is involved in the uptake of gadoxetic acid in HCC cells. Narita et al (29) recently reported similar results to ours. They also verified that there was a significant correlation between the enhancement ratio in the hepatobiliary phase and the expression level of OATP1B3 (synonymous with OATP8 [20]) protein at Western blot analysis in HCCs. However, their study focused solely on OATP1B3 and did not analyze the involvement of any other transporters. Therefore, the mechanisms of transporters in gadoxetic acid uptake were not elucidated in their entirety. We examined other possible transporters, because transporters can compensate to some extent for the functions of others, especially in disrupted conditions. Indeed, OATP8 and OATP-C share 80% of their amino acid sequences, and can transport some common substrates into cells (17). In our study, we showed that OATP8 and MRP3 expression correlated with enhancement ratio in HCCs, whereas the other five transporters containing OATP-C showed no significant correlations. However, it may be that the expression level does not always correspond with the functional level of a transporter. To examine the functional levels of OATP8 and the other transporters, further studies using cultures of purified hepatocytes from hypointense and iso- or hyperintense HCCs are needed.

MRP3 is an export transporter of organic anions on the sinusoidal side of hepatocytes. Its expression was significantly increased in iso- or hyperintense HCCs, which means that the excretion of gadoxetic acid from HCC cells into the tumor blood spaces (tumor sinusoids) is enhanced, probably because of the depletion of bile ducts in HCCs. We surmise this to be a reactive response to the increase in OATP8 expression, to export more substrate into blood. In contrast, the excretion by MRP2, the transporter on the canalicular side, would not function in HCCs, because there are few larger bile ducts in tumor tissue. Therefore, the efflux of gadoxetic acid into tumor blood spaces would appear to be the main route of excretion from HCC cells in iso- or hyperintense HCCs. The rate of excretion is likely to be slower than the rate of uptake and thus to hardly influence the SI in the hepatobiliary phase of gadoxetic acid–enhanced MR imaging.

We also analyzed the histologic differences between hypointense HCCs and iso- or hyperintense HCCs. The majority of iso- or hyperintense HCCs were moderately differentiated HCCs; this may be due to genetic reversion to their original hepatocyte nature during hepatocarcinogenesis because, as shown by Tsuda et al (30), the ability of tumor cells to take up gadoxetic acid would be expected to be lost during the early stage of hepatocarcinogenesis in rats. Interestingly, iso- or hyperintense HCCs showed pseudoglandular proliferation

Figure 6

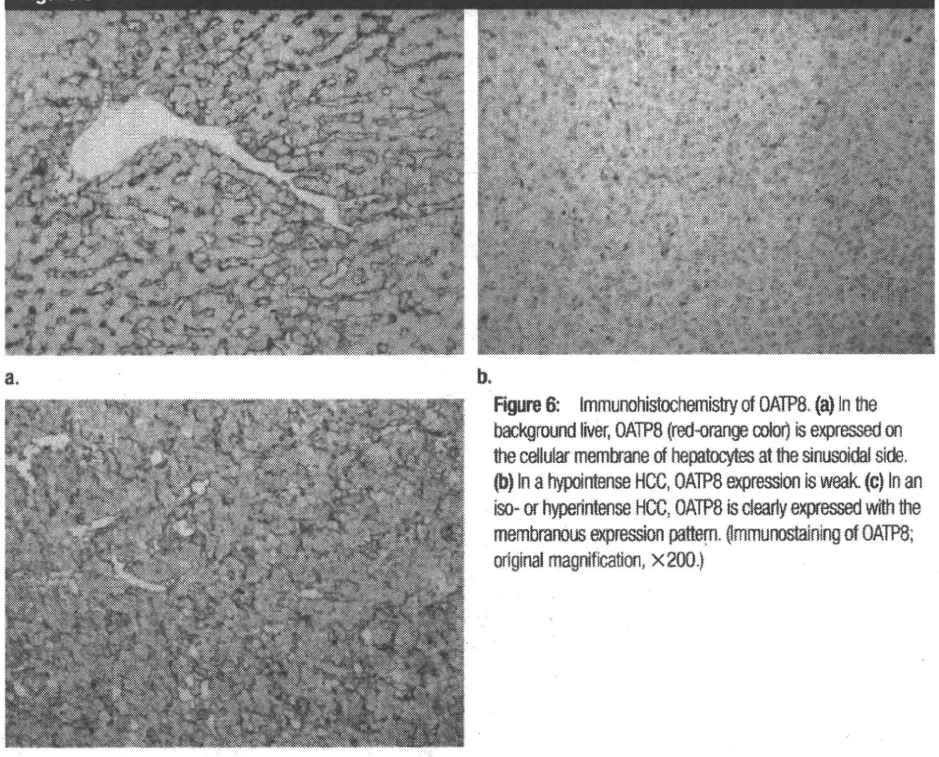

Figure 6: Immunohistochemistry of OATP8. **(a)** In the background liver, OATP8 (red-orange color) is expressed on the cellular membrane of hepatocytes at the sinusoidal side. **(b)** In a hypointense HCC, OATP8 expression is weak. **(c)** In an iso- or hyperintense HCC, OATP8 is clearly expressed with the membranous expression pattern. (Immunostaining of OATP8; original magnification, ×200.)

Figure 7

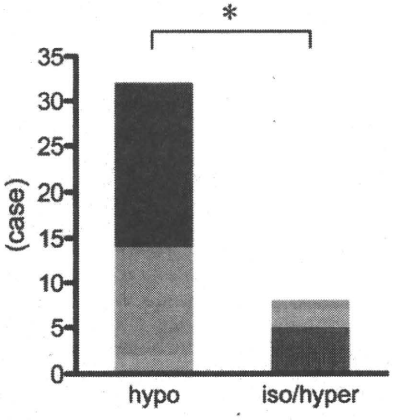

Figure 7: Bar graph shows results of semiquantitative analysis of the immunohistochemistry of OATP8. OATP8 expression in iso- or hyperintense HCCs *(iso/hyper)* is significantly extensive compared with that in hypointense HCCs *(hypo)* (* = $P < .001$, Mann-Whitney test). Blue = no expression, green = decreased expression, yellow = equivalent expression, red = increased expression.

with bile plugs with significantly high frequency, suggesting overproduction of bile and secondary dilatation of bile canaliculi (31). Overexpression of OATP8 might contribute to the overproduction of bile, because OATP8 can take up bile acid components. However, this proliferation pattern was also fairly often seen in hypointense HCCs. It is difficult to directly correlate the expression levels of OATP8 and the quantity of bile production, because nonanion transporters such as Na^+/taurocholate cotransporting polypeptide and organic cation transporter also participate in bile production (32).

Benign hepatocellular nodules, like focal nodular hyperplasia, commonly show isointensity or hyperintensity in the hepatobiliary phase (4–6). We suppose that uptake transporters, including OATP8 and export transporters, are expressed normally or increasingly in these hyperplastic cells. However, the SI may be determined by the expression of uptake transporters rather than that of export transporters, as shown in our study. Radiologic-pathologic studies of benign or premalignant hepatocellular nodules performed with similar methods are needed to clarify this issue.

Our study had several limitations. First, the total number of iso- or hyperintense HCCs examined was small because such tumors are relatively rare, and reverse transcription PCR was performed in only 22 of 40 HCCs from which we could obtain fresh-frozen specimens. Second, we simply divided HCCs into hypointense and iso- or hyperintense type according to the average SI in the maximum ROI for this analysis. In the future, it will be important to correlate each area of different SI with tumor differentiation, proliferation pattern, or the expression of transporters in heterogeneous lesions. However, we believe that the data obtained are sufficient to make conclusions about the molecular biology of gadoxetic acid–enhanced MR imaging pharmacodynamics, because the expression levels

Figure 8

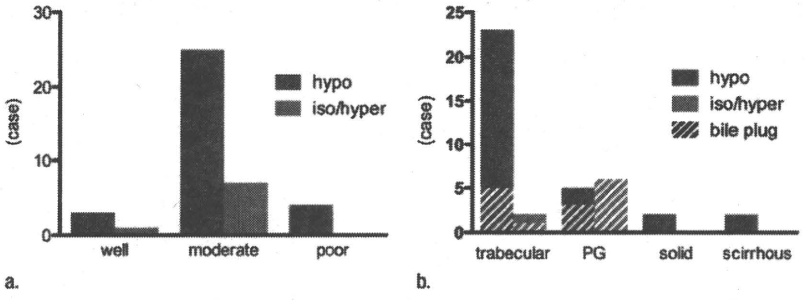

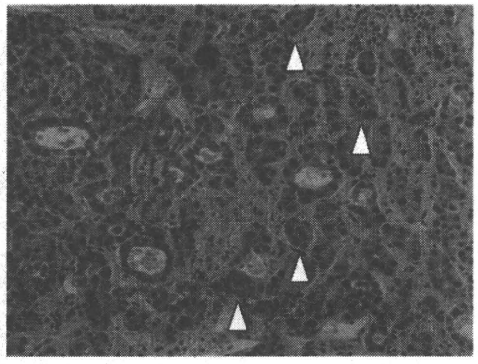

c.

Figure 8: Histologic proliferation patterns of HCCs. **(a)** Graph shows tumor differentiation. The hypointense HCCs *(hypo)* consisted of well-differentiated (9%), moderately differentiated (78%), and poorly differentiated HCCs (12%), while 88% of iso- or hyperintense HCCs *(iso/hyper)* were moderately differentiated. **(b)** Graph shows tumor proliferation pattern. Seventy-five percent of iso- or hyperintense HCCs had a pseudoglandular pattern, and 88% showed bile plugs. In the hypointense HCCs, the trabecular pattern was most common; in addition, a pseudoglandular *(PG)* proliferation pattern and bile production were observed in 19% and 31% of nodules, respectively. There was no significant difference in tumor differentiation ($P = .57$), while there were significant differences in proliferation patterns or bile production between the two types of HCCs ($P = .01$ and $P = .006$, respectively). **(c)** A case of iso- or hyperintense HCC shows a pseudoglandular pattern with bile production (arrowheads). (Hematoxylin-eosin stain; original magnification, ×200.)

Figure 9

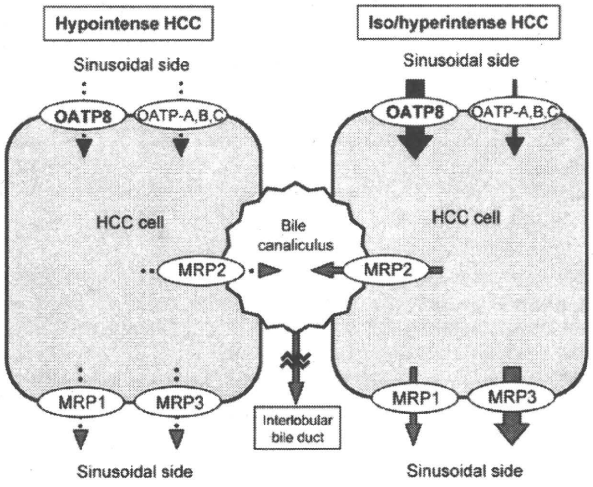

Figure 9: Schematic of transporter expression and mechanism of gadoxetic acid dynamics in HCC. Between hypointense and iso- or hyperintense HCCs, the most significant differences were observed in OATP8 and MRP3 expression. That is, in iso- or hyperintense HCCs, a larger amount of gadoxetic acid would be taken up from the tumor blood sinusoids into HCC cells by OATP8 and be excreted again into tumor blood sinusoids by MRP3 very gradually, probably because of the depletion of bile ducts in the HCCs. In contrast, in hypointense HCCs, the uptake of gadoxetic acid might be blocked or reduced because of the lower expression of OATP8.

of OATP8 and MRP3 and the time-SI curves showed significant differences between the two types of HCCs. Third, patients with poor liver function were not included in this study. The relative SI in the hepatobiliary phase would be modified in these patients; for example, HCC without OATP8 expression could be visualized as isointense. Therefore, the liver function of patients should be considered when evaluating the SI of HCCs (33,34).

In conclusion, the expression of the uptake transporter OATP8 and the export transporter MRP3 in HCC cells significantly correlated with the SI of HCCs in the hepatobiliary phase of gadoxetic acid–enhanced MR imaging. In human HCC cells, OATP8 and MRP3 are probably the uptake transporter and export transporter of gadoxetic acid, respectively.

References

1. Vogl TJ, Kümmel S, Hammerstingl R, et al. Liver tumors: comparison of MR imaging with Gd-EOB-DTPA and Gd-DTPA. Radiology 1996;200(1):59–67.

2. Huppertz A, Balzer T, Blakeborough A, et al. Improved detection of focal liver lesions at MR imaging: multicenter comparison

of gadoxetic acid-enhanced MR images with intraoperative findings. Radiology 2004; 230(1):266–275.

3. Bluemke DA, Sahani D, Amendola M, et al. Efficacy and safety of MR imaging with liver-specific contrast agent: U.S. multicenter phase III study. Radiology 2005;237(1):89–98.
4. Huppertz A, Haraida S, Kraus A, et al. Enhancement of focal liver lesions at gadoxetic acid-enhanced MR imaging: correlation with histopathologic findings and spiral CT—initial observations. Radiology 2005; 234(2):468–478.
5. Zech CJ, Herrmann KA, Reiser MF, Schoenberg SO. MR imaging in patients with suspected liver metastases: value of liver-specific contrast agent Gd-EOB-DTPA. Magn Reson Med Sci 2007;6(1):43–52.
6. Reimer P, Schneider G, Schima W. Hepatobiliary contrast agents for contrast-enhanced MRI of the liver: properties, clinical development and applications. Eur Radiol 2004; 14(4):559–578.
7. Saito K, Kotake F, Ito N, et al. Gd-EOB-DTPA enhanced MRI for hepatocellular carcinoma: quantitative evaluation of tumor enhancement in hepatobiliary phase. Magn Reson Med Sci 2005;4(1):1–9.
8. Schuhmann-Giampieri G, Schmitt-Willich H, Press WR, Negishi C, Weinmann HJ, Speck U. Preclinical evaluation of Gd-EOB-DTPA as a contrast agent in MR imaging of the hepatobiliary system. Radiology 1992;183(1):59–64.
9. Hamm B, Staks T, Mühler A, et al. Phase I clinical evaluation of Gd-EOB-DTPA as a hepatobiliary MR contrast agent: safety, pharmacokinetics, and MR imaging. Radiology 1995;195(3):785–792.
10. Hecht EM, Holland AE, Israel GM, et al. Hepatocellular carcinoma in the cirrhotic liver: gadolinium-enhanced 3D T1-weighted MR imaging as a stand-alone sequence for diagnosis. Radiology 2006;239(2):438–447.
11. Reimer P, Rummeny EJ, Daldrup HE, et al. Enhancement characteristics of liver metastases, hepatocellular carcinomas, and hemangiomas with Gd-EOB-DTPA: preliminary results with dynamic MR imaging. Eur Radiol 1997;7(2):275–280.
12. Bartolozzi C, Crocetti L, Lencioni R, Cioni D, Della Pina C, Campani D. Biliary and reticuloendothelial impairment in hepatocarcinogenesis: the diagnostic role of tissue-specific MR contrast media. Eur Radiol 2007; 17(10):2519–2530.
13. van Montfoort JE, Stieger B, Meijer DK, Weinmann HJ, Meier PJ, Fattinger KE. Hepatic uptake of the magnetic resonance imaging contrast agent gadoxetate by the organic anion transporting polypeptide Oatp1. J Pharmacol Exp Ther 1999;290(1): 153–157.
14. Lorusso V, Pascolo L, Fernetti C, Visigalli M, Anelli P, Tiribelli C. In vitro and in vivo hepatic transport of the magnetic resonance imaging contrast agent B22956/1: role of MRP proteins. Biochem Biophys Res Commun 2002;293(1):100–105.
15. Abe T, Kakyo M, Tokui T, et al. Identification of a novel gene family encoding human liver-specific organic anion transporter LST-1. J Biol Chem 1999;274(24): 17159–17163.
16. Hsiang B, Zhu Y, Wang Z, et al. A novel human hepatic organic anion transporting polypeptide (OATP2). Identification of a liver-specific human organic anion transporting polypeptide and identification of rat and human hydroxymethylglutaryl-CoA reductase inhibitor transporters. J Biol Chem 1999;274(52):37161–37168.
17. König J, Cui Y, Nies AT, Keppler D. Localization and genomic organization of a new hepatocellular organic anion transporting polypeptide. J Biol Chem 2000;275(30): 23161–23168.
18. Kullak-Ublick GA, Ismair MG, Stieger B, et al. Organic anion-transporting polypeptide B (OATP-B) and its functional comparison with three other OATPs of human liver. Gastroenterology 2001;120(2):525–533.
19. Kullak-Ublick GA, Hagenbuch B, Stieger B, et al. Molecular and functional characterization of an organic anion transporting polypeptide cloned from human liver. Gastroenterology 1995;109(4):1274–1282.
20. Vavricka SR, Jung D, Fried M, Grützner U, Meier PJ, Kullak-Ublick GA. The human organic anion transporting polypeptide 8 (SLCO1B3) gene is transcriptionally repressed by hepatocyte nuclear factor 3beta in hepatocellular carcinoma. J Hepatol 2004;40(2): 212–218.
21. Zhou SF, Wang LL, Di YM, et al. Substrates and inhibitors of human multidrug resistance associated proteins and the implications in drug development. Curr Med Chem 2008; 15(20):1981–2039.
22. Müller M, Roelofsen H, Jansen PL. Secretion of organic anions by hepatocytes: involvement of homologues of the multidrug resistance protein. Semin Liver Dis 1996;16(2): 211–220.
23. Tsujii H, König J, Rost D, Stöckel B, Leuschner U, Keppler D. Exon-intron organization of the human multidrug-resistance protein 2 (MRP2) gene mutated in Dubin-Johnson syndrome. Gastroenterology 1999; 117(3):653–660.
24. König J, Rost D, Cui Y, Keppler D. Characterization of the human multidrug resistance protein isoform MRP3 localized to the basolateral hepatocyte membrane. Hepatology 1999;29(4):1156–1163.
25. Zech CJ, Vos B, Nordell A, et al. Vascular enhancement in early dynamic liver MR imaging in an animal model: comparison of two injection regimen and two different doses Gd-EOB-DTPA (gadoxetic acid) with standard Gd-DTPA. Invest Radiol 2009;44(6): 305–310.
26. Terminology of nodular hepatocellular lesions. International Working Party. Hepatology 1995;22(3):983–993.
27. Hirohashi S, Ishak KG, Kojiro M, et al. Hepatocellular carcinoma. In: Hamilton SR, Aaltonen LA, eds. Pathology and genetics of tumours of the digestive system. Lyon, France: IARC, 2000; 157–172.
28. Nakamura K, Zen Y, Sato Y, et al. Vascular endothelial growth factor, its receptor Flk-1, and hypoxia inducible factor-1alpha are involved in malignant transformation in dysplastic nodules of the liver. Hum Pathol 2007;38(10):1532–1546.
29. Narita M, Hatano E, Arizono S, et al. Expression of OATP1B3 determines uptake of Gd-EOB-DTPA in hepatocellular carcinoma. J Gastroenterol 2009;44(7):793–798.
30. Tsuda N, Kato N, Murayama C, Narazaki M, Yokawa T. Potential for differential diagnosis with gadolinium-ethoxybenzyl-diethylenetriamine pentaacetic acid-enhanced magnetic resonance imaging in experimental hepatic tumors. Invest Radiol 2004;39(2):80–88.
31. Kondo Y, Nakajima T. Pseudoglandular hepatocellular carcinoma. A morphogenetic study. Cancer 1987;60(5):1032–1037.
32. Kullak-Ublick GA, Beuers U, Paumgartner G. Hepatobiliary transport. J Hepatol 2000; 32(1 suppl):3–18.
33. Ryeom HK, Kim SH, Kim JY, et al. Quantitative evaluation of liver function with MRI Using Gd-EOB-DTPA. Korean J Radiol 2004;5(4):231–239.
34. Kim T, Murakami T, Hasuike Y, et al. Experimental hepatic dysfunction: evaluation by MRI with Gd-EOB-DTPA. J Magn Reson Imaging 1997;7(4):683–688.

Hepatocarcinogenesis: Multistep Changes of Drainage Vessels at CT during Arterial Portography and Hepatic Arteriography—Radiologic-Pathologic Correlation[1]

Azusa Kitao, MD
Yoh Zen, MD
Osamu Matsui, MD
Toshifumi Gabata, MD
Yasuni Nakanuma, MD

Purpose: To clarify the changes that occur in drainage vessels of dysplastic nodules and hepatocellular carcinoma (HCC) during hepatocarcinogenesis by using computed tomography (CT) during arterial portography (CTAP) and CT during hepatic arteriography (CTHA), with histologic findings as the reference standard.

Materials and Methods: Institutional ethics committee approval and informed consent were obtained. According to the findings at CTAP and CTHA, 46 surgically resected hepatocellular nodules were classified into three types: type A (n = 18) (equivalent or decreased portal perfusion compared with background liver at CTAP, decreased arterial perfusion, and no corona enhancement [perinodular contrast material drainage] at CTHA), type B (n = 13) (no portal perfusion, increased arterial perfusion, and thin (≤2-mm) corona enhancement), or type C (n = 15) (no portal perfusion, increased arterial perfusion, and thick (>2-mm) corona enhancement). We compared the histopathologic features and microangioarchitecture between the types.

Results: Type A nodules histologically consisted of dysplastic nodules and well-differentiated HCC; type B and C nodules were moderately differentiated HCC. Replacing growth was commonly observed in type A nodules, whereas compressing growth was more frequently seen in types B and C. Sixty percent of type C nodules had a fibrous capsule. There were significantly fewer intranodular hepatic veins in types B and C. Serial pathologic slices demonstrated continuity from intranodular capillarized sinusoids to hepatic veins in type A nodules and to surrounding hepatic sinusoids in type B nodules. In type C nodules, intranodular capillarized sinusoids were connected to extranodular portal veins either directly or through portal venules within the fibrous capsule.

Conclusion: Drainage vessels of HCC change from hepatic veins to hepatic sinusoids and then to portal veins during multistep hepatocarcinogenesis.

[1] From the Departments of Radiology (A.K., O.M., T.G.) and Human Pathology (A.K., Y.Z., Y.N.), Kanazawa University Graduate School of Medical Science, 13-1 Takaramachi, Kanazawa 920-8640, Japan. Received August 10, 2008; revision requested September 24; revision received January 7, 2009; accepted March 2; final version accepted March 16. Supported in part by Grant-in-Aid for Cancer Research (no. 18S-01) from Ministry of Health, Labor, and Welfare and by Health and Labor Sciences Research Grants for Development of Novel Molecular Markers and Imaging Modalities for Earlier Diagnosis of Hepatocellular Carcinoma. **Address correspondence to** A.K. (e-mail: *kitao@rad.m.kanazawa-u.ac.jp*).

Hepatocellular carcinoma (HCC) is usually associated with chronic liver disease, especially chronic viral hepatitis and liver cirrhosis (1,2). HCC has been proved to develop by multistep carcinogenesis from a dysplastic nodule (DN), to early HCC (highly well-differentiated HCC), and finally to overt hypervascular HCC (moderately differentiated HCC) (3–10).

To understand the pathophysiology of HCC, especially in its early stage, the multistep changes in the blood supply of DNs and HCC have been well studied with radiologic techniques (11,12). Computed tomography (CT) during arterial portography (CTAP) and CT during hepatic arteriography (CTHA) are useful radiologic methods for evaluating in vivo dynamics of portal supply and arterial supply, respectively, in hepatic lesions (11–17). DNs show the same or mildly decreased portal perfusion at CTAP and decreased arterial perfusion at CTHA compared with surrounding liver parenchyma. On the other hand, moderately differentiated HCC shows no portal perfusion at CTAP and clearly increased arterial perfusion at CTHA. In brief, the inflow of nodules changes from a mainly portal supply to an exclusively arterial supply during the multistep hepatocarcinogenesis (12). These radiologic findings reflect the histologic vascular structure of HCC (18,19).

Advances in Knowledge

- The main drainage vessels of hepatocellular carcinoma (HCC) change from hepatic veins to hepatic sinusoids to portal veins during multistep hepatocarcinogenesis.
- The thickness of corona enhancement (perinodular drainage of contrast material) of HCC at late-phase CT during hepatic arteriography correlates with the histologic grade of tumor malignancy and the type of drainage vessels.
- The changes in HCC drainage vessels could be triggered by the early reduction of intranodular hepatic veins owing to tumor invasion.

In comparison to inflow, little attention has been paid to drainage flow of HCC and DNs, although a few radiologic studies regarding drainage vessels of HCC have been published (20–22). Ueda et al (22) used single-level dynamic CTHA to clarify the drainage vessels of hypervascular HCC with a fibrous capsule. In their study, intranodular contrast enhancement was observed, and subsequently, perinodular enhancement with bright branching structures appeared on single-level dynamic CTHA images. They concluded that perinodular enhancement, named *corona enhancement*, is the drainage area of the tumor and that the branching structures are portal venules corresponding to the drainage route. However, the radiologic-pathologic correlation has not been fully elucidated. In particular, how the drainage vessels change during multistep hepatocarcinogenesis has not been examined.

In our study, we tried to clarify the changes that occur in drainage vessels during hepatocarcinogenesis from DN to moderately differentiated HCC. We evaluated intranodular and perinodular hemodynamics by using CTAP and CTHA, with a focus on the correlation of corona enhancement at late-phase CTHA with histopathologic features.

Materials and Methods

Patients

This retrospective study was performed with the approval of the institutional ethics committee, and informed consent was obtained from patients. It focused on 46 hepatocellular nodules in 40 patients, which were surgically resected and were pathologically diagnosed as DNs or HCC at our institution between 1998 and 2007. We did not include large (>6 cm in diameter) nodules or poorly differentiated HCCs, because they are often associated with secondary changes that might influence imaging (eg, necrosis, hemorrhage, invasion of the portal or hepatic veins). All patients (mean age, 61.0 years ± 8.4 [standard deviation]; men, 85%; women, 15%) had chronic liver disease. No patient had previously undergone treatment (eg, ablation therapy, transarterial chemoembolization therapy, chemotherapy) for hepatocellular nodules.

Implications for Patient Care

- The grade of tumor malignancy may be indicated by analyzing corona enhancement of HCC at dynamic CT, dynamic MR imaging, or contrast-enhanced US.
- Knowledge of venous drainage is important for understanding the pathophysiology of HCC and for precise performance of interventional therapy or surgical resection.

CTAP and CTHA

Both CTAP and CTHA were performed in all patients before surgical resection (mean time before surgery, 41.3 days ± 17.8) because of their extremely high sensitivity for detection of other nodular lesions (11). CTAP and CTHA were performed with various CT scanners (XVision SP, Toshiba Medical Systems, Tokyo, Japan; Aquilion 64, Toshiba Medical Systems; HiSpeed Advantage, GE Healthcare, Milwaukee, Wis; and LightSpeed Ultra 16, GE Healthcare). From the femoral artery, 4-F catheters were inserted into the superior mesenteric artery for CTAP and into

Published online
10.1148/radiol.2522081414

Radiology 2009; 252:605–614

Abbreviations:
CTAP = CT during arterial portography
CTHA = CT during hepatic arteriography
DN = dysplastic nodule
HCC = hepatocellular carcinoma

Author contributions:
Guarantors of integrity of entire study, all authors; study concepts/study design or data acquisition or data analysis/interpretation, all authors; manuscript drafting or manuscript revision for important intellectual content, all authors; approval of final version of submitted manuscript, all authors; literature research, A.K., O.M.; clinical studies, A.K., Y.Z., O.M., T.G., Y.N.; statistical analysis, A.K.; and manuscript editing, A.K., Y.Z., O.M., Y.N.

Authors stated no financial relationship to disclose.

the common, proper, or replaced right hepatic artery for CTHA.

CTAP scans were obtained at 5–7-mm section thickness and 5–7-mm collimation to cover the entire liver in a single breath hold. To increase the blood flow and decrease the laminar flow of the portal vein, 5 μg of prostaglandin E1 (Palux; Taisho, Tokyo, Japan) was injected into the superior mesenteric artery before contrast material infusion. Helical scanning began 25 seconds after the infusion of 50–70 mL of iohexol (320–350 milligrams of iodine per milliliter) (Omnipaque; Daiichi, Tokyo, Japan) at a rate of 1.8 mL/sec by using a power injector was started.

CTHA scans were obtained at 3–5-mm section thickness and 3–5-mm collimation. Helical scanning was started 7 seconds after the beginning of an infusion of iohexol (320–350 milligrams of iodine per milliliter) into the common, proper, or replaced hepatic artery at a rate of 1.8 mL/sec. The infusion of contrast material was continued until 5 seconds after early-phase CTHA scanning was completed. The scanning time varied according to the individual liver size (about 20–25 seconds). The total amount of contrast medium varied according to the following equation: (early-phase scanning time + 12 seconds) × injection rate. Thirty seconds after contrast material infusion finished (about 62–67 seconds after the infusion began), late-phase scanning commenced.

Figure 1

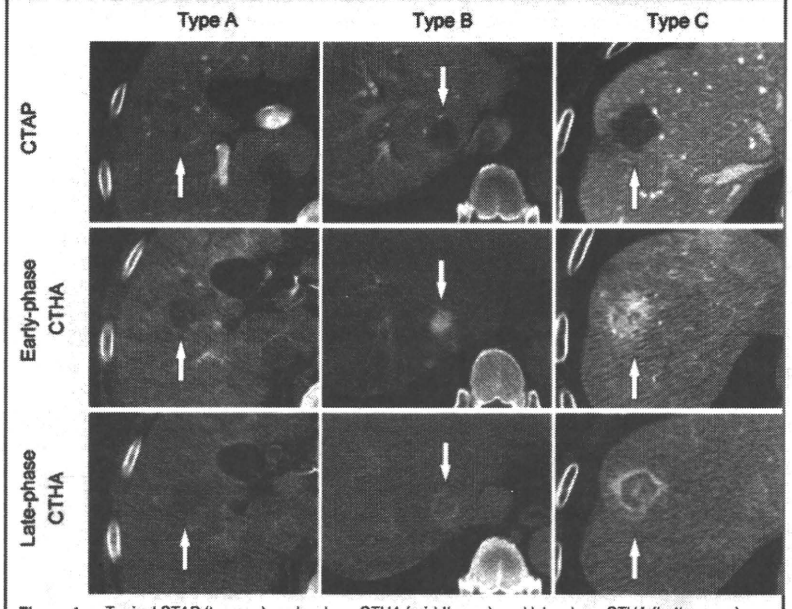

Figure 1: Typical CTAP (top row), early-phase CTHA (middle row), and late-phase CTHA (bottom row) findings for the three nodule types (arrows). Type A nodule (left column) has equivalent-to-decreased portal perfusion on CTAP imaging, decreased arterial perfusion on early-phase CTHA images, and no corona enhancement on late-phase CTHA images. Type B nodule (middle column) has portal perfusion defect and increased arterial perfusion with thin corona enhancement. Type C nodule (right column) has portal perfusion defect, increased arterial perfusion, and thicker corona enhancement.

Radiologic Classification of Hepatocellular Nodules

The nodules were retrospectively classified into three types according to the findings at CTAP and CTHA in consensus by two radiologists (A.K. and O.M., with 8 and 38 years experience, respectively) who were blinded to any pathologic information. The classifications were determined on the basis of past reports about the findings of CTAP and CTHA.

We defined a type A nodule as a nodular lesion that showed equivalent or decreased portal perfusion as compared with background liver on CTAP images, decreased arterial perfusion compared with background liver on early-phase CTHA images, and no perinodular stain-

Clinical Features by Tumor Type

Clinical Feature	Type A	Type B	Type C
No. of tumors	18	13	15
Resected tumor size (cm)*	2.0 ± 1.2 (0.9–4.8)	2.7 ± 1.6 (1.2–5.2)	2.6 ± 1.2 (1.6–5.5)
Age (y)*	58.9 ± 6.6 (47–70)	62.6 ± 8.9 (53–71)	62.7 ± 9.6 (53–76)
Male-to-female ratio	14:4	10:3	14:1
Underlying disease process			
Chronic hepatitis	6	3	6
Hepatitis B virus	2	0	1
Hepatitis C virus	4	3	4
Hepatitis B and C viruses	0	0	1
Liver cirrhosis	12	10	9
Hepatitis B virus	3	4	5
Hepatitis C virus	7	5	3
Cryptogenic	2	1	1

Note.—Unless otherwise specified, data are numbers of patients.
* Data are means ± standard deviations, with ranges in parentheses.

ing corona enhancement on late-phase CTHA images. Type B nodules showed no portal perfusion, clearly increased arterial perfusion compared with background liver, and thin corona enhancement. Thin corona enhancement was defined as flat perinodular enhancement on late-phase CTAP images that was less than or equal to 2 mm thick. Type C nodules showed no portal perfusion, clearly increased arterial perfusion compared with background liver, and thick corona enhancement on late-phase CTHA images. Thick corona enhancement was defined as perinodular enhancement with or without irregular protrusions that was greater than 2 mm thick. We set this 2-mm threshold because we clinically observed that smooth or flat corona enhancement was exclusively less than 2 mm thick, and in contrast, irregular or protruding corona enhancement was almost always more than 2 mm thick.

Type A nodules corresponded to DNs or well-differentiated HCCs, and type B and C nodules were part of well-differentiated HCCs or, mainly, moderately differentiated HCCs (11–17). There was no case that showed apparent reduction of portal perfusion of the liver on CTAP images. Typical CTAP and CTHA findings for the three types of nodules are shown in Figure 1.

Pathologic Examinations

Liver specimens were fixed with neutral formalin, and 4-mm-thick paraffin-embedded tissue slices were prepared from each nodule. Hematoxylin-eosin staining was performed. To clearly differentiate each vessel, double immuno-

Figure 2

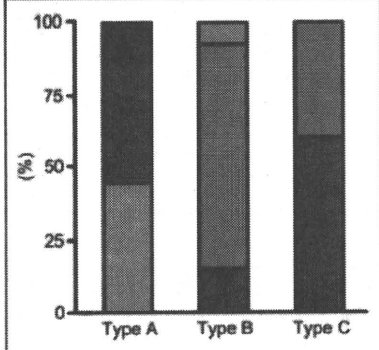

Figure 2: Bar graph of percentage of each tumor differentiation grade by tumor type. Blue = DN ($n = 10$), green = well-differentiated HCC ($n = 9$), orange = moderately differentiated HCC without fibrous capsule ($n = 16$), red = moderately differentiated HCC with fibrous capsule ($n = 11$).

Figure 3

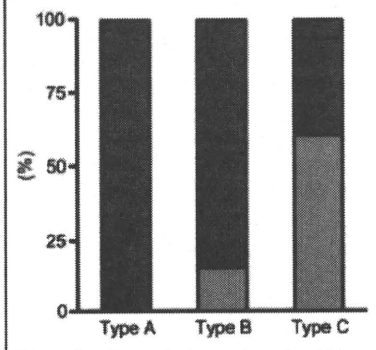

Figure 3: Bar graph of percentage of each histologic growth pattern by tumor type. Blue = replacing growth, red = compressing growth without fibrous capsule, green = compressing growth with fibrous capsule.

Figure 4

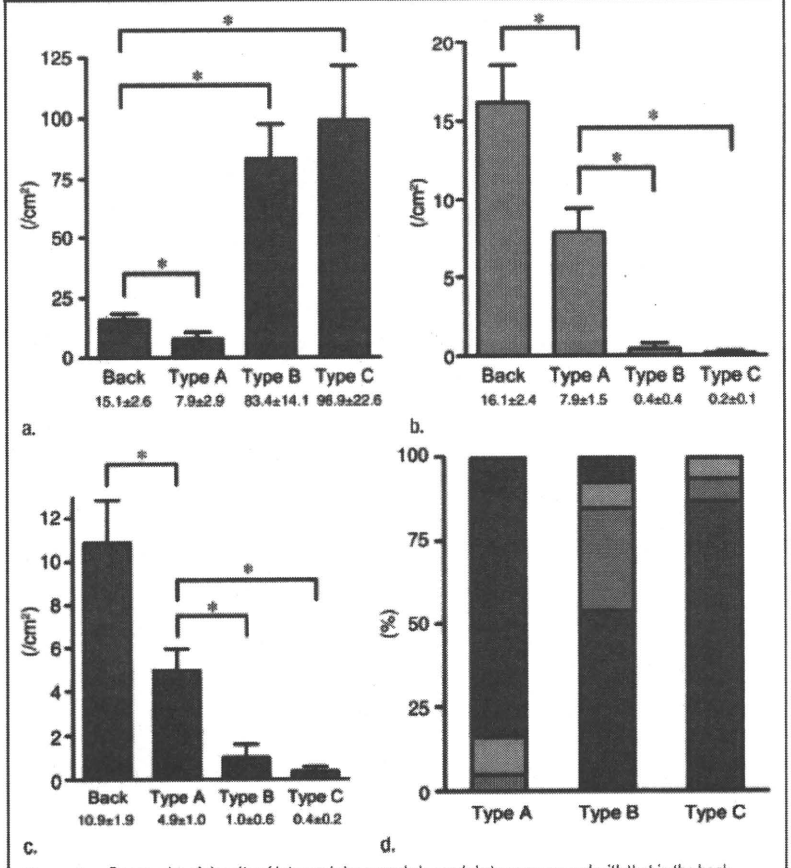

Figure 4: Bar graphs of density of intranodular vessels by nodule type compared with that in the background liver tissue *(Back)* for **(a)** arteries, **(b)** portal vein, and **(c)** hepatic vein. Mean value ± standard deviation is given under each bar. * = $P < .05$ with multiple comparison test. **(d)** Bar graph of percentage of area of capillarized sinusoids by nodule type shows progressive increase in percentage of capillarized area in type A versus type B versus type C nodules ($P < .05$ with Kruskal-Wallis test). Blue = 1+, green = 2+, orange = 3+, red = 4+.

Figure 5

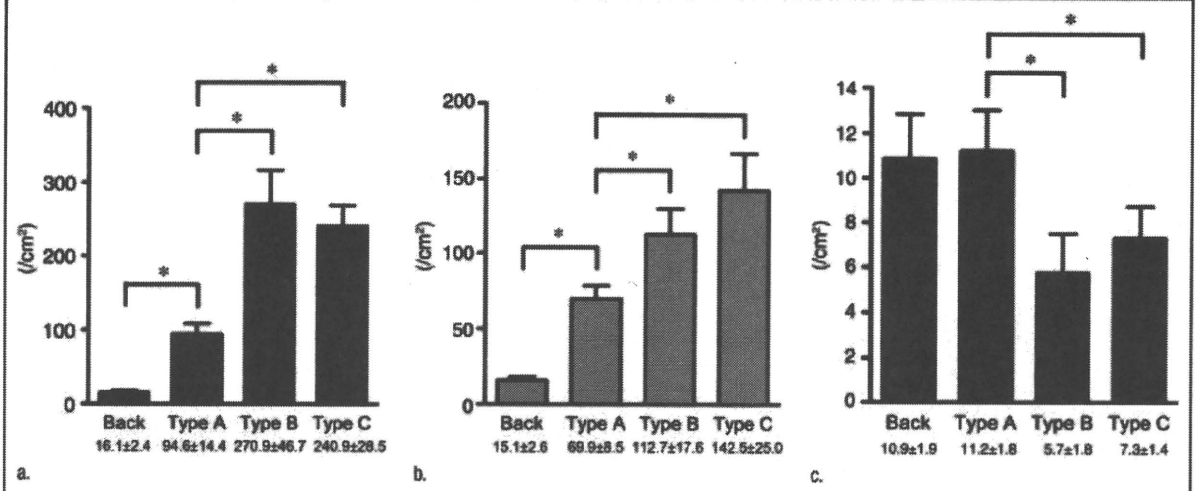

Figure 5: Bar graphs of density of perinodular vessels by nodule type compared with that in the background liver tissue *(Back)* for **(a)** arteries, **(b)** portal vein, and **(c)** hepatic vein. Mean value ± standard deviation is given under each bar. * = $P < .05$ with **(a, b)** multiple comparison or **(c)** unpaired *t* test.

staining with CD34 (a vascular endothelial cell marker) and α-smooth muscle actin (a smooth muscle cell marker) was performed in all nodules. Two pathologists (Y.Z. and Y.N., with 11 and 37 years experience, respectively) and one radiologist (A.K.), who were blinded to all imaging information, evaluated the three nodule types in consensus for tumor differentiation, fibrous capsule formation, tumor growth pattern, background liver tissue (chronic hepatitis or liver cirrhosis), and number of vessels.

Tumor differentiation and fibrous capsule.—We classified each nodule into one of four grades for tumor differentiation according to the classifications proposed by the International Working Party (8) and the World Health Organization (23): DN, well-differentiated HCC, moderately differentiated HCC without fibrous capsule, and moderately differentiated HCC with fibrous capsule. A DN was defined as a small nodular lesion of hepatocytes with mild nuclear and cytoplasmic atypia, cellular density increase, and no evidence of malignancy (eg, stromal or vessel invasion). In our study, the DN category included both low- and high-grade DNs because they both show similar findings on CTAP and CTHA images (17). Well-differentiated HCC was de-

Figure 6

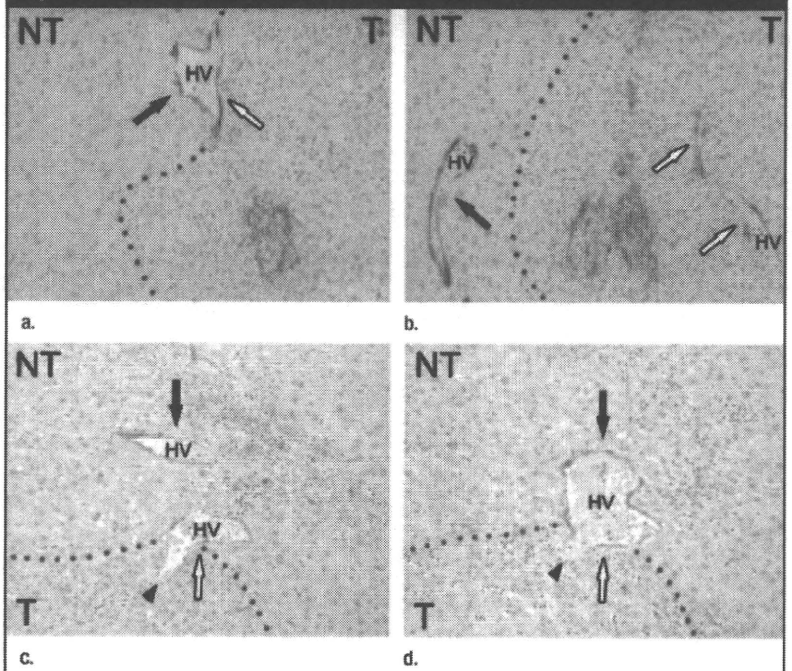

Figure 6: Serial pathologic slices show continuity of vessels at the border (dotted line) of a type A nodule (DN). **(a, b)** Intranodular preexisting hepatic vein (*HV*, white arrows) and extranodular hepatic veins (black arrows). **(c, d)** Intranodular capillarized sinusoid (arrowheads) continues into hepatic vein (white arrows) at nodule border and then into extranodular hepatic vein (black arrows). *NT* = not tumor, *T* = tumor. (Double immunostaining with CD34 [brown] and α-smooth muscle actin [red]; magnification, ×200.)

Figure 7

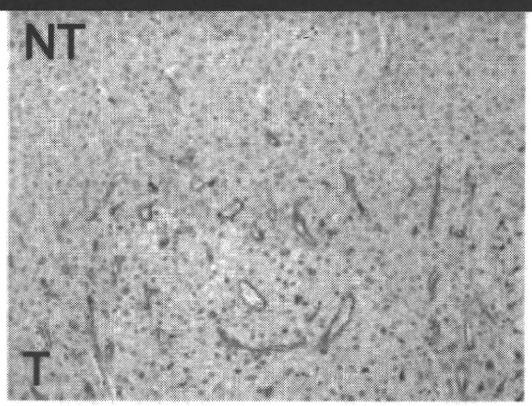

Figure 7: Continuities of intranodular capillarized sinusoids (brown) and extranodular hepatic sinusoids are diffusely observed at the border of a type B nodule (moderately differentiated HCC with replacing growth). *NT* = not tumor, *T* = tumor. (CD34 and α–smooth muscle actin; magnification, ×200.)

Figure 8

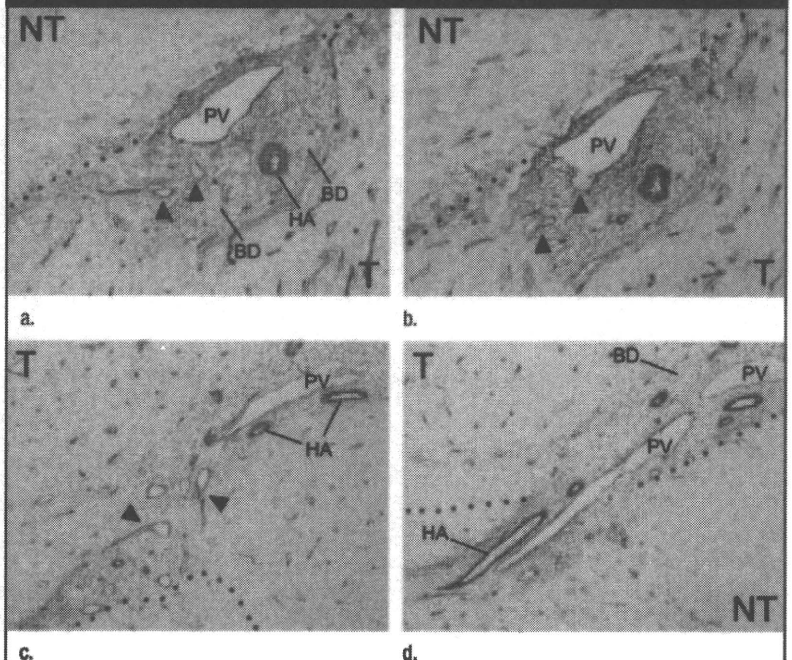

Figure 8: Continuities of vessels at border (dotted line) of a type C nodule (moderately differentiated HCC without fibrous capsule). Intranodular capillarized sinusoids (arrowheads) connect to extranodular portal veins *(PV)* **(a, b)** directly and **(c, d)** indirectly (through portal venules within the fibrous septum). Portal venules are accompanied by hepatic arteries *(HA)* and bile ducts *(BD)*. *NT* = not tumor, *T* = tumor. (CD34 and α–smooth muscle actin; magnification, ×200.)

fined as a nodular lesion consisting of malignant hepatocytes that showed evident nuclear and cytoplasmic atypia and higher cellular density. Intranodular portal tracts were relatively preserved. Moderately differentiated HCC was composed of malignant hepatocytes proliferating in trabecular, pseudoglandular, and solid patterns. We defined a fibrous capsule as fibrous tissue that was greater than 0.2 mm thick and surrounded more than two-thirds of the tumor circumference.

Tumor growth pattern.—Nodule growth patterns were classified into two types: replacing and compressing. In the nodules with replacing growth, tumor cells proliferated by replacing surrounding hepatic parenchyma, and the margin between nodules and background liver tissue was indistinct. Compressing-growth nodules had a discrete margin and pushed out the surrounding hepatic parenchyma.

Underlying disease process.—For each nodule type, we compared the proportion of patients with chronic hepatitis with that of patients with liver cirrhosis to analyze the influence of the underlying disease process on background liver tissue.

Number of vessels.—We counted the numbers of vessels twice. The number of arteries (both hepatic and neovascularized unpaired arteries), portal veins, and hepatic veins were counted in three areas: within tumor parenchyma, not including the fibrous septa or fibrous capsule; in the perinodular area less than 2 mm from the nodule border; and in the background liver away from the nodule. Intranodular and background liver vessels were counted in the largest square we could draw in the respective areas of the tissue slices. Perinodular vessels were counted in 10 random fields within 2 mm of the tumor border (magnification, ×100) or within as many fields as possible on small slices. Then, we divided the number of vessels by the area to calculate vessel density (per square centimeter).

We also measured the area of intranodular capillarized sinusoids covered by endothelial cells expressing CD34 and compared it with the whole

area of the nodule in the same slice (18,24). Capillarized area in each nodule was semiquantitatively rated as follows: 1+ = 0%–25%, 2+ = 26%–50%, 3+ = 51%–75%, and 4+ = 76%–100%.

Continuity of vessels at nodule border.—To clarify the continuity between intranodular vascular structures and extranodular drainage vessels at the border of the nodule, more than 200 serial slices were prepared from one tumor of each type (ie, A, B, and C). By using double immunostaining with CD34 and α-smooth muscle actin, we examined continuities between intranodular and extranodular vascular structures on serial slices.

Statistical Analysis

The data were expressed as means ± standard deviations. Statistical significance was evaluated by using the Kruskal-Wallis test for the comparison of tumor differentiation, tumor growth pattern, and the area of intranodular capillarized sinusoids; unpaired *t* test for the comparison of the number of perinodular hepatic veins between tumor types; and multiple comparison test (Dunnet procedure) for the analysis of the number of other vessels. *P* values less than .05 were considered to indicate statistical significance.

Results

Clinical Features by Nodule Type

Eighteen nodules were classified as type A; 13, as type B; and 15, as type C. The clinical features of the patients and the tumor sizes are listed by type in the Table. As determined from resected specimens, the mean size of all hepatocellular nodules was 2.4 cm ± 1.3.

Pathologic Features by Nodule Type

Tumor differentiation and fibrous capsule.—At histologic analysis (Fig 2), type A nodules consisted of 10 DNs and eight well-differentiated HCCs. Type B nodules comprised one well-differentiated HCC and 12 (92%) moderately differentiated HCCs, 10 (83%) of which did not have a fibrous capsule. All 15 type C nodules were moderately differentiated HCCs, nine (60%) of which had a fibrous capsule (Kruskal-Wallis test, $P < .05$).

Figure 9

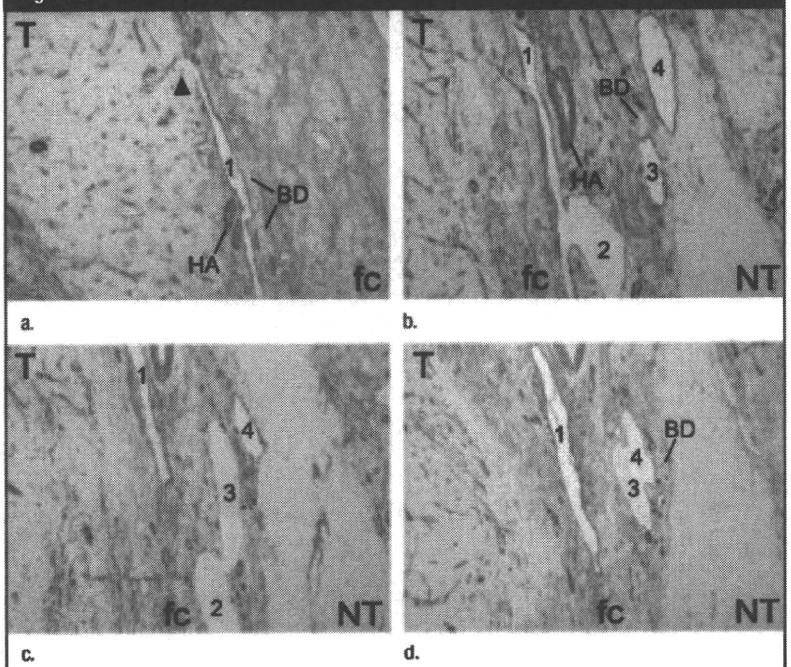

Figure 9: **(a–d)** Continuities of vessels at the border of a type C nodule (moderately differentiated HCC with fibrous capsule *[fc]*). Intranodular capillarized sinusoid (arrowhead, **a**) connects to portal venules (*1*, **a**) and drains into extranodular portal veins (*1–4*, **b–d**). *BD* = bile duct, *HA* = hepatic arteries, *NT* = not tumor, *T* = tumor. (CD34 and α-smooth muscle actin; magnification, ×100.)

Tumor growth pattern.—Histologic growth patterns for each type are shown in Figure 3. All of the type A nodules showed a replacing growth pattern. Half of type B nodules had replacing growth, and the other half had compressing growth. Almost all type C nodules (93%) showed compressing growth (Kruskal-Wallis test, $P < .05$). The proportion of nodules with compressing pattern was higher in type C than in type B (93% vs 54%).

Underlying disease process.—No significant difference with regard to histologic findings in the liver was observed between the three types of nodules. The percentages of chronic hepatitis and liver cirrhosis were 33% versus 67%, respectively, for type A nodules; 23% versus 77%, respectively, for type B nodules; and 33% versus 67%, respectively, for type C nodules.

Intranodular vessels.—Compared with the that in the background liver, the density of intranodular arteries was decreased in type A nodules and increased in type B and C nodules (all $P < .05$) (Fig 4). There was no statistically significant difference in the density of arteries between type B and C nodules. The density of intranodular portal veins was also decreased in type A nodules compared with the background liver and was decreased in type B and C nodules compared with type A nodules (all $P < .05$). The density of hepatic veins was similarly decreased ($P < .05$). The percentage of the nodule occupied by intranodular capillarized sinusoids progressively increased in type A versus B versus C nodules (Fig 4).

Perinodular vessels.—As shown in Figure 5, the density of perinodular arteries and portal veins was increased in type A nodules compared with the back-

ground liver ($P < .05$ with the multiple comparison test). In addition, type B and C nodules had higher densities of arteries and portal veins than did type A nodules ($P < .05$ with the multiple comparison test). In contrast, the density of hepatic veins around type B and C nodules was decreased compared with type A nodules ($P < .05$ with unpaired t test). No significant difference was observed in the density of any perinodular vessels between type B and type C nodules ($P < .05$).

Continuity of vessels at nodule border.—In the type A nodule, which was a DN, serial pathologic slices revealed the continuity between intranodular preexisting hepatic veins and extranodular hepatic veins (Fig 6a, 6b). In addition, intranodular capillarized sinusoids continued into extranodular hepatic veins (Fig 6c, 6d).

We also examined the serial pathologic slices of a type B nodule, which was a moderately differentiated HCC without a fibrous capsule that had a replacing growth pattern, for continuity of intranodular capillarized sinusoids and surrounding hepatic sinusoids (Fig 7). Intranodular and perinodular hepatic veins were rarely observed; therefore, their continuity was not confirmed.

We used two type C moderately differentiated HCCs to examine the continuity of vessels at the tumor border. One demonstrated compressing growth without a fibrous capsule, and the other showed compressing growth with a fibrous capsule. We observed many portal venules within the intranodular fibrous septa and the fibrous capsule, accompanied by hepatic arteries and bile ducts. In the nodule without a fibrous capsule, intranodular capillarized sinusoids connected to extranodular portal veins directly (Fig 8a, 8b). In addition, intranodular capillarized sinusoids connected to portal venules within the fibrous septum, and these portal venules continued into extranodular portal veins (Fig 8c, 8d). In the nodule with a fibrous capsule, intranodular capillarized sinusoids connected to portal venules within the fibrous capsule, with these venules connecting to extranodular portal veins (Fig 9).

Figure 10

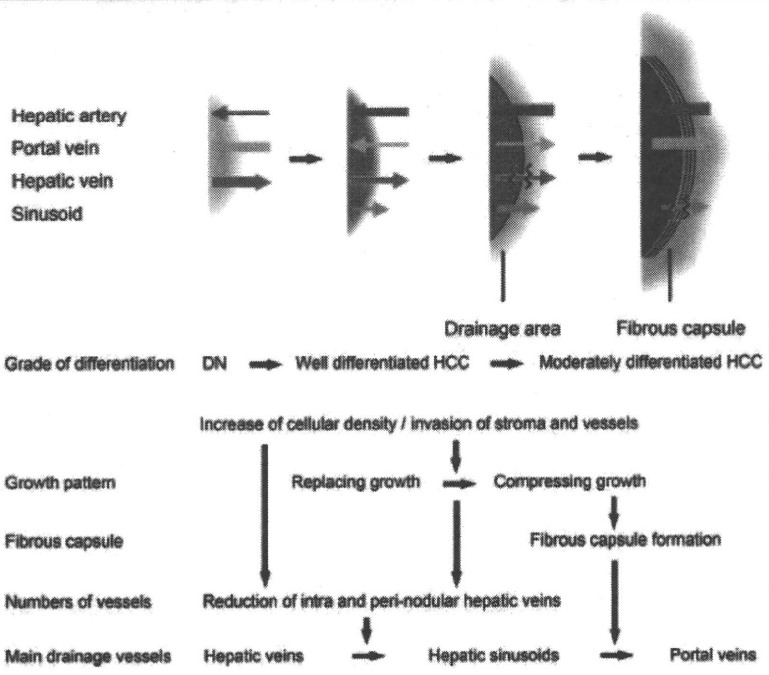

Figure 10: Diagram of the mechanism underlying changes in drainage vessels (top) and histologic features (bottom) of HCC during multistep hepatocarcinogenesis. Top: Direction of arrow = direction of flow for that vessel type. Thickness of arrow = volume through that vessel. Wavy lines through arrow = disruption of flow. Gray area = nodule.

Discussion

The different radiologic appearances of type A, B, and C nodules seem to be the direct result of several histologic features: the grade of tumor differentiation, fibrous capsule formation, and tumor growth pattern. According to the theory of multistep hepatocarcinogenesis, we think that these histologic features change as the nodules progress from type A (DN or well-differentiated HCC) to type B to type C (both moderately differentiated HCC). The results of our study suggest that the main drainage vessels change from hepatic veins (type A) to hepatic sinusoids (type B) and then to portal veins (type C) during this progression.

On the basis of our findings, a mechanism for how the drainage vessels of HCC change during multistep hepatocarcinogenesis can be postulated (Fig 10). As the tumor cells become more atypical and proliferate more rapidly, they first invade the intranodular hepatic veins because they are not accompanied by fibrous tissue (eg, Glisson's sheath surrounding portal veins). In the perinodular area, hepatic veins are similarly collapsed by tumor compression. Therefore, intranodular and perinodular hepatic veins disappear earlier than do portal veins. When the drainage through hepatic veins is blocked, drainage flows mainly into surrounding hepatic sinusoids and partially into portal veins according to the blood pressure gradient. As the intranodular cellular density increases, the tumor growth pattern changes from replacing growth to compressing growth, and a thick fibrous capsule is formed by the compressed perinodular liver tissue (25). At this stage, perinodular hepatic sinusoids are collapsed, and the conti-

nuity of intranodular and extranodular sinusoids is interrupted by fibrous capsule formation. Therefore, drainage blood flow has no outlet other than through portal veins, accompanied by a marked increase in arterial blood supply. Although the total number of intranodular portal veins is decreased, portal venules are relatively well preserved in the fibrous septa and capsule. These patent portal venules could become the drainage vessels of an established encapsulated HCC.

The direction of hepatic arterial flow is afferent, while that of hepatic venous flow is efferent owing to the pressure gradient. In contrast, the direction of portal flow to nodules is variable and can be determined by using the combination of CTAP and histologic findings. Type C nodules showed no portal perfusion at CTAP, and direct connections between intranodular capillarized sinusoids and portal venules were confirmed with histologic findings. We believe that the direction of portal flow would be efferent in type C nodules. That is, blood flow in portal veins seems to dramatically change during multistep hepatocarcinogenesis from afferent flow in type A nodules to efferent flow in type C nodules.

Previously, perinodular contrast enhancement was thought to represent the presence of a fibrous capsule (26,27). However, as shown in type C nodules, corona enhancement was frequently broader than the histologically confirmed fibrous capsule and included a protruding portion. Moreover, corona enhancement was also seen in nonencapsulated type B and C HCC nodules. Therefore, we conclude that corona enhancement consists of staining of mainly the perinodular parenchyma, although it might contain staining of the fibrous capsule, as well. However, the drainage area of type B nodules was thinner and smoother than that of type C nodules. This difference might be explained by the fact that the draining blood pressure or speed through surrounding hepatic sinusoids (type B nodules) might be lower than that through portal veins (type C nodules). Drainage area of type A nodules could not be observed because contrast material drained directly into the hepatic vein and did not pass through perinodular hepatic sinusoids. The corona enhancement findings at late-phase CTHA are surmised to closely correlate with the histologic changes of drainage vessels.

As has been previously reported (11–17), pathologic changes of arteries and portal veins in DNs and HCC are closely correlated with the radiologic findings. We should keep in mind that the background liver previous studies and ours used as the control does not represent normal liver (mainly chronic liver disease). In comparison to background liver, type A nodules had decreased intranodular arteries, and types B and C had significantly increased intranodular arteries and capillarized sinusoids. The findings on early-phase CTHA images reflected the histologic findings. In contrast, the density of intranodular portal veins decreased from type A to type B and C nodules, which corresponds to the findings on CTAP images.

In addition, we found an interesting pathologic feature; similar to intranodular portal veins, the density of intranodular hepatic veins markedly decreased from type A to type B and C nodules. Density of perinodular hepatic veins was also decreased in type B and C nodules, probably owing to tumor compression, whereas the densities of perinodular portal veins and hepatic arteries were increased. As mentioned above, hepatic veins might more readily collapse than would portal veins because of the absence of perivascular connective tissue. This impairment of blood flow through the hepatic veins could possibly trigger the dramatic change of drainage blood flow into the portal veins.

On the basis of the radiologic findings of our study, particularly corona enhancement, imaging can be used to provide insight into the grade of malignancy or drainage vessels of hepatocellular nodules. Drainage vessels seem to be a main factor in determining tumor progression, therefore understanding the drainage routes of HCC has implications for interventional therapy (eg, transarterial chemoembolization or ablation) and surgical resection (18,28). At transarterial chemoembolization of hypervascular HCCs, outflow of iodized oil into perinodular portal veins or surrounding parenchyma is often observed (29,30). This finding suggests that the drainage vessels are portal veins or sinusoids. Nodule drainage has been shown to influence the treatment efficacy of transarterial chemoembolization (31).

Our study had several limitations. First, serial slices of only four nodules were used to evaluate the continuity of vessels at the nodule border. In the remaining nodules the drainage route was surmised from the number of vessels in the tumor and surrounding liver in correlation with the CTAP and CTHA findings. Second, quantitative analysis of all drainage vessels was not feasible. Therefore, in the case of mixed drainage routes (eg, portal veins and surrounding hepatic sinusoids), the main route could not be accurately determined. However, we do not believe these factors negate the new concept proposed in our study.

In conclusion, the main drainage vessels of hepatocellular nodules change from hepatic veins to surrounding hepatic sinusoids and then to portal veins during multistep hepatocarcinogenesis. This change seems to be triggered by the early disappearance of intranodular and perinodular hepatic veins. This notion is important for understanding pathophysiologic and radiologic features of DN, early HCC, and moderately differentiated HCC.

References

1. Villa E, Baldini GM, Pasquinelli C, et al. Risk factors for hepatocellular carcinoma in Italy: male sex, hepatitis B virus, non-A non-B infection, and alcohol. Cancer 1988;62:611–615.

2. Unoura M, Kaneko S, Matsushita E, et al. High-risk groups and screening strategies for early detection of hepatocellular carcinoma in patients with chronic liver disease. Hepatogastroenterology 1993;40:305–310.

3. Takayama T, Makuuchi M, Hirohashi S, et al. Malignant transformation of adenomatous hyperplasia to hepatocellular carcinoma. Lancet 1990;336:1150–1153.

4. Sakamoto M, Hirohashi S, Shimosato Y. Early stages of multistep hepatocarcinogenesis: adenomatous hyperplasia and early hepatocellular carcinoma. Hum Pathol 1991;22:172–178.

5. Kobayashi M, Ikeda K, Hosaka T, et al. Dysplastic nodules frequently develop into hepatocellular carcinoma in patients with chronic viral hepatitis and cirrhosis. Cancer 2006; 106:636–647.

6. Nakanuma Y, Terada T, Terasaki S, et al. Atypical adenomatous hyperplasia in liver cirrhosis: low-grade hepatocellular carcinoma or borderline lesion? Histopathology 1990;17:27–35.

7. Nakanuma Y, Terada T, Ueda K, Terasaki S, Nonomura A, Matsui O. Adenomatous hyperplasia of the liver as a precancerous lesion. Liver 1993;13:1–9.

8. Terminology of nodular hepatocellular lesions: International Working Party. Hepatology 1995;22:983–993.

9. Nakashima O, Sugihara S, Kage M, Kojiro M. Pathomorphologic characteristics of small hepatocellular carcinoma: a special reference to small hepatocellular carcinoma with indistinct margins. Hepatology 1995; 22:101–105.

10. Nakano M, Saito A, Yamamoto M, Doi M, Takasaki K. Stromal and blood vessel wall invasion in well-differentiated hepatocellular carcinoma. Liver 1997;17:41–46.

11. Matsui O, Kadoya M, Kameyama T, et al. Benign and malignant nodules in cirrhotic livers: distinction based on blood supply. Radiology 1991;178:493–497.

12. Hayashi M, Matsui O, Ueda K, Kawamori Y, Gabata T, Kadoya M. Progression to hypervascular hepatocellular carcinoma: correlation with intranodular blood supply evaluated with CT during intraarterial injection of contrast material. Radiology 2002;225:143–149.

13. Matsui O, Takashima T, Kadoya M, et al. Dynamic computed tomography during arterial portography: the most sensitive examination for small hepatocellular carcinomas. J Comput Assist Tomogr 1985;9:19–24.

14. Takayasu K, Muramatsu Y, Furukawa H, et al. Early hepatocellular carcinoma: appearance at CT during arterial portography and CT arteriography with pathologic correlation. Radiology 1995;194:101–105.

15. Murakami T, Takamura M, Kim T, et al. Double phase CT during hepatic arteriography for diagnosis of hepatocellular carcinoma. Eur J Radiol 2005;54:246–252.

16. Tajima T, Honda H, Taguchi K, et al. Sequential hemodynamic change in hepatocellular carcinoma and dysplastic nodules: CT angiography and pathologic correlation. AJR Am J Roentgenol 2002;178:885–897.

17. Hayashi M, Matsui O, Ueda K, et al. Correlation between the blood supply and grade of malignancy of hepatocellular nodules associated with liver cirrhosis: evaluation by CT during intraarterial injection of contrast medium. AJR Am J Roentgenol 1999;172:969–976.

18. Park YN, Yang CP, Fernandez GJ, Cubukcu O, Thung SN, Theise ND. Neoangiogenesis and sinusoidal "capillarization" in dysplastic nodules of the liver. Am J Surg Pathol 1998; 22:656–662.

19. Ueda K, Terada T, Nakanuma Y, Matsui O. Vascular supply in adenomatous hyperplasia of the liver and hepatocellular carcinoma: a morphometric study. Hum Pathol 1992;23: 619–626.

20. Toyosaka A, Okamoto E, Mitsunobu M, Oriyama T, Nakao N, Miura K. Intrahepatic metastases in hepatocellular carcinoma: evidence for spread via the portal vein as an efferent vessel. Am J Gastroenterol 1996;91: 1610–1615.

21. Tochio H, Kudo M. Afferent and efferent vessels of premalignant and overt hepatocellular carcinoma: observation by color Doppler imaging. Intervirology 2004;47:144–153.

22. Ueda K, Matsui O, Kawamori Y, et al. Hypervascular hepatocellular carcinoma: evaluation of hemodynamics with dynamic CT during hepatic arteriography. Radiology 1998;206:161–166.

23. Hirohashi S, Ishak KG, Kojiro M, et al. Hepatocellular carcinoma. In: Hamilton SR, Aaltonen LA, eds. Pathology and genetics of tumours of the digestive system. Lyon, France: IARC, 2000; 157–172.

24. Nakamura K, Zen Y, Sato Y, et al. Vascular endothelial growth factor, its receptor Flk-1, and hypoxia inducible factor-1alpha are involved in malignant transformation in dysplastic nodules of the liver. Hum Pathol 2007;38:1532–1546.

25. Okuda K, Musha H, Nakajima Y, et al. Clinicopathologic features of encapsulated hepatocellular carcinoma: a study of 26 cases. Cancer 1977;40:1240–1245.

26. Ros PR, Murphy BJ, Buck JL, Olmedilla G, Goodman Z. Encapsulated hepatocellular carcinoma: radiologic findings and pathologic correlation. Gastrointest Radiol 1990; 15:233–237.

27. Lim JH, Choi D, Park CK, Lee WJ, Lim HK. Encapsulated hepatocellular carcinoma: CT-pathologic correlations. Eur Radiol 2006;16: 2326–2333.

28. Sakon M, Nagano H, Nakamori S, et al. Intrahepatic recurrence of hepatocellular carcinoma after hepatectomy. Arch Surg 2002; 137:94–99.

29. Matsui O, Kadoya M, Yoshikawa J, et al. Small hepatocellular carcinoma: treatment with subsegmental transcatheter arterial embolization. Radiology 1993;188:79–83.

30. Terayama N, Matsui O, Gabata T, et al. Accumulation of iodized oil within the nonneoplastic liver adjacent to hepatocellular carcinoma via the drainage routes of the tumor after transcatheter arterial embolization. Cardiovasc Intervent Radiol 2001;24:383–387.

31. Miyayama S, Matsui O, Yamashiro M, et al. Ultraselective transcatheter arterial chemoembolization with a 2-f tip microcatheter for small hepatocellular carcinomas: relationship between local tumor recurrence and visualization of the portal vein with iodized oil. J Vasc Interv Radiol 2007;18:365–376.